ELSEVIER

International Journal of Heat and Fluid Flow 22 (2001) 227–236

International Journal of HEAT AND FLUID FLOW

www.elsevier.com/locate/ijhff

Simultaneous measurements of concentration and velocity in a CO_2 jet issuing into a grid turbulence by two-sensor hot-wire probe

Yasuhiko Sakai [a,*], Takao Watanabe [b], Satoru Kamohara [a], Takehiro Kushida [a], Ikuo Nakamura [c]

[a] *Department of Mechano-informatics and Systems, Nagoya University, Furo-cho, Chikusa-ku, Nagoya 464-8603, Japan*
[b] *Kawasaki Heavy Industries, Ltd, Tokyo Head Office: World Trade Center Building, 4-1, Hamamatsu-cho, 2-chome, Minato-ku, Tokyo 105-6116, Japan*
[c] *Department of Mechanical System Engineering, Meijo University, Shiogamaguchi 1-501, Tenpaku-ku, Nagoya 468-8502, Japan*

Abstract

A new simple method has been developed to measure the concentration and velocity simultaneously for the gas mixture (CO_2–air) flow by two hot-wire probes. By using a calibration map, the values of the instantaneous concentration and velocity can be determined from the voltages of two hot-wire probes with different overheat ratios (OHR) by digital data processing. This method does not require subtle adjustment of the OHR to achieve insensitivity to the CO_2 concentration, as in the past work by Chassaing (Mélange turbulent de gaz inertes dans un jet tube libre, Thèse Doc. Sciences 42, Inst. Nat. Poly. de Toulouse, 1979). The measurements have been performed in a CO_2 jet in grid turbulence. The experimental results for the centerline and radial distributions of the mean and r.m.s. values of mass fraction concentration and velocity, and axial scalar flux are consistent with previous data. © 2001 Published by Elsevier Science Inc.

Keywords: CO_2-air mixture; Two hot-wire probe; Volumetric concentration; Mass fraction concentration; Velocity; Simultaneous measurements; Jet; Grid turbulence

1. Introduction

In this paper, we describe a simple new technique for the simultaneous measurements of fluctuating concentration and velocity of CO_2–air mixtures using a composite probe consisting of two hot-wire sensors. This work is the first step for the simultaneous measurements of concentration and two-components of velocity (velocity components parallel and perpendicular to the mainstream direction). In the past, excellent work for the simultaneous measurements of concentration and velocity has been reported. For example, Way and Libby (1971) developed a composite probe consisting of a hot-wire and hot-film sensor which thermally interfere. They showed that the concentration and velocity of helium–air mixtures could be determined from the two voltages of the hot-wire and hot-film sensor. This method, however, is useful only for gases of large heat conductivity such as helium. On the other hand, for CO_2 (which has a relatively small conductivity), Chassaing (1979) suggested another composite probe consisting of two parallel hot-wire sensors with different overheat ratios (hereafter the overheat ratio is abbreviated to 'OHR'). He found the existence of an OHR for which the sensitivity of one hot-wire to the CO_2 concentration vanishes. This means that the velocity can be measured independently of the CO_2 concentration by using this hot wire insensitive to the concentration. Chassaing (1979) further checked the dependency of another hot-wire voltage on the CO_2 concentration, then performed simultaneous measurements of concentration and velocity of the CO_2–air mixtures. However, we should notice that Chassaing's method leads to some practical difficulty in adjusting the OHR of one hot wire appropriately so as to eliminate its concentration sensitivity. We here propose a simple new method in which the adjustment of the OHR of one hot-wire sensor is unnecessary, and report the results of the actual simultaneous measurements of mass fraction concentration and velocity in a CO_2 jet issued in a grid turbulence as an experimental example.

2. Principle of simultaneous measurements by two hot-wire probes

2.1. Theoretical consideration of wire voltage in gas flow

If the wire heated by the electric current I in a steady flow is in thermal equilibrium, the relation between the Joule's heat W

* Corresponding author. Tel.: +81-52-789-4488; fax: +81-52-789-3111.
E-mail address: ysakai@mech.nagoya-u.ac.jp (Y. Sakai).

0142-727X/01/$ - see front matter © 2001 Published by Elsevier Science Inc.
PII: S0142-727X(01)00084-4

Notation

b	temperature coefficient of electric resistance
C_p	specific heat at constant pressure
d	diameter of hot wire or diameter of jet exit
d_{eff}	effective diameter of jet exit, $d_{eff} = d_{in}^{p}(\rho_J/\rho_0)^{0.5}$
d_{in}^{p}	inner diameter of CO_2 issuing pipe
d_{out}^{p}	outer diameter of CO_2 issuing pipe
E	voltage across hot wire
E_1, E_2	voltages across hot wire at low and high overheat ratios (OHR)
F, f	Mean and fluctuating mass fraction concentration of CO_2
H	heat loss from hot wire per unit time
h	heat transfer coefficient
I	electric heating current
l	length of hot wire
Nu	Nusselt number
Pr	Prandtl number
Re	Reynolds number
R_w	electric resistance of hot wire
R_0	electric resistance of hot wire at ambient fluid temperature
T_w	hot wire temperature
T_0	ambient fluid temperature
T_m	mean film temperature, $T_m = (T_w + T_0)/2$
U, u	mean and fluctuating velocity
U_x, u_x	mean and fluctuating velocity in x-direction for jet
U_0	mean streamwise velocity in grid turbulent flow
W	Joule's heat of hot wire per unit time
X	downstream distance from grid
X_M	downstream distance of virtual origin from grid
x, r	axial and radial coordinates for jet

Greeks

Γ, γ	mean and fluctuating volumetric concentration of CO_2
ε_T	temperature OHR, $\varepsilon_T = (T_w - T_0)/T_0$
ε_R	resistance OHR, $\varepsilon_R = (R_w - R_0)/R_0$
ρ	density
λ	heat conductivity
μ	viscosity
ν	kinetic viscosity, $\nu = \mu/\rho$

Subscripts

c	quantity on jet centerline
J	quantity at jet exit
0	quantity concerning ambient fluid
air	quantity concerning air
CO_2	quantity concerning CO_2

Superscript

$'$	root mean square value

and the heat loss H per unit time is $W = H$. Since $W = I^2R_w$, where the resistance of the wire is R_w, we obtain

$$I^2R_w = H. \tag{1}$$

If all the heat loss from the circular cylinder is due to the heat transfer by the forced convection alone, the heat loss can be expressed as follows:

$$H = hS(T_w - T_0). \tag{2}$$

Here the heat transfer coefficient is h (W/(m^2 K)), the heating surface area is $S = \pi dl$ (m^2) (d and l are wire diameter, wire length, respectively), and the wire temperature and the ambient gas temperature are T_w (K) and T_0 (K), respectively. With the introduction of the Nusselt number Nu ($= hd/\lambda$, λ is the heat conductivity of the gas (W/(m K))), the thermal equilibrium of the wire gives the following equation:

$$I^2R_w = \pi d\lambda(T_w - T_0)Nu. \tag{3}$$

The Nusselt number depends on various other dimensionless parameters [Reynolds number $Re = Ud/\nu$, Prandtl number $Pr = C_p\mu/\lambda$ (C_p: specific heat at constant pressure), OHR ε_T (defined by Eq. (9)), etc.]. This dependence is too complicated to be determined theoretically. Therefore, the expression of Nu can be empirically obtained from experiments. Kramers (1946) suggested the following empirical relation from the data of water, air, and three kinds of oils, which cover $0.71 < Pr < 525$, $0.1 < Re < 1.0 \times 10^4$:

$$Nu = 0.42\,Pr^{0.20} + 0.57\,Pr^{0.33}\,Re^{0.50}. \tag{4}$$

In air, the following Collis and Williams (1959) equation is widely accepted for $Re < 44$:

$$Nu = (T_m/T_0)^{0.7}\left(0.24 + 0.56\,Re^{0.45}\right), \tag{5}$$

where T_m is the mean film temperature defined by $T_m = (T_w + T_0)/2$. On the other hand, Wu and Libby (1971) suggested a modified version of Eq. (5) for air, helium and a mixture of the two gases. The modified equation is given by

$$Nu = (T_m/T_0)^{0.7}\left[0.24\{Pr/(Pr)_{air}\}^{0.20} + 0.56\{Pr/(Pr)_{air}\}^{0.33}\,Re^{0.45}\right], \tag{6}$$

where Pr and $(Pr)_{air}$ denote the Prandtl number for the gas and air at the mean film temperature T_m. Further, Simpson and Wyatt (1973) have investigated the heat loss of various hot films in air, helium and argon and in helium–air and argon–air mixtures. These authors used Eq. (5) as a basis for analysis of their results. Although it was necessary to allow the numerical constants (0.24 and 0.56) in Eq. (5) to be parameters and determine them experimentally, they would obtain an excellent correction of their experimental data with the resulting equation.

At present, an expression of Nu valid for all the gases and different OHRs is not available (Pitts and McCaffrey, 1986). However, Eq. (6) is very simple, so that here we use Eq. (6) to proceed with our discussions on the simultaneous measurement of the species concentration and velocity for gas–air mixture flow.

The temperature dependence of R_w may be expressed as follows:

$$R_w \fallingdotseq R_0[1 + b(T_w - T_0)], \tag{7}$$

where b is the constant coefficient ($b = 5.2 \times 10^{-3}$ K^{-1} for the tungsten, $b = 3.5 \times 10^{-3}$ K^{-1} for the platinum) and R_0 is the resistance of the wire at the gas temperature T_0. Let the heating voltage be E, and from Eqs. (3), (6) and (7), we obtain

$$E^2 \fallingdotseq \pi l\lambda(T_w - T_0)R_0\{1 + b(T_w - T_0)\}(T_m/T_0)^{0.7} \times \left[0.24\{Pr/(Pr)_{air}\}^{0.20} + 0.56\{Pr/(Pr)_{air}\}^{0.33}\,Re^{0.45}\right]. \tag{8}$$

Eq. (8) indicates that the voltage across the hot wire is dependent on the wire temperature (or OHR) and properties as

well as the velocities of the cooling fluid. From Eq. (8), we notice that the simultaneous use of two hot wires with different OHRs provides two signals from which the instantaneous species concentration and velocity can be determined for an isothermal mixture flow. This is the basis for the present simultaneous measurements of the concentration and velocity for gas–air flow by two-sensor hot-wire probe.

2.2. Prediction of hot-wire voltage

We adopted Eq. (8) to predict the hot-wire voltages in the CO_2 and air flow. Substituting the physical properties (λ, Pr) of CO_2 and air at $T_m = 400$, 500, 600 K ($T_m = (T_0 + T_w)/2$) into Eq. (8), we predicted the relations between E_2^2 and U. The physical properties were cited from Katayama (1986). If T_0 is assumed to be 288 K, T_w are 512, 712, 912 K for the above values of T_m, respectively. Then, the temperature OHRs defined by

$$\varepsilon_T = (T_w - T_0)/T_0 \tag{9}$$

correspond to 0.77, 1.47 and 2.17, respectively. Further, we assumed that the platinum wire length $l = 1$ mm, the diameter $d = 5$ μm, and the resistance at T_0, $R_0 = 5.4$ Ω. Fig. 1 shows the prediction results in these conditions. From Fig. 1, we find that in case of the small ε_T, the wire voltage in the CO_2 gas flow is smaller than one in the air flow. However, as ε_T becomes larger, the difference between two wire voltages become small, then the relation between two voltages will be inverse. It is noticed that in case of $\varepsilon_T = 1.47$, the difference between two voltages is very small, so that the sensitivity of the wire to the concentration almost vanishes. If we can reduce the difference between two voltages completely to zero by adjusting appropriately the OHR of one hot-wire sensor, this hot-wire probe cannot perceive the change in concentration. Therefore, by using this probe, the flow velocity can be measured independently of any CO_2 concentration. If the above insensitive hot-wire probe is combined with another probe sensitive to the concentration, simultaneous measurements become possible. This method was actually performed by Chassaing (1979).

2.3. Calibrations of two hot-wire probes in CO_2 flow and air flow

In this paper, the mean volumetric concentration of CO_2 and its fluctuation are denoted by Γ and γ, and % is used as a unit of the volumetric concentration. On the other hand, the mean and fluctuation mass fraction concentration are denoted by F and f. A tilde indicates the instantaneous total values of these quantities. The relation between the instantaneous volumetric concentration $\tilde{\Gamma}$ and mass fraction concentration $\tilde{F}$ is given as follows (Warnatz et al., 1999):

$$\tilde{F} = \frac{M_{CO_2}\tilde{\Gamma}}{M_{CO_2}\tilde{\Gamma} + M_{air}(100 - \tilde{\Gamma})}, \tag{10}$$

where M_{CO_2} and M_{air} are molar weights for CO_2 and air, respectively. These values are given by $M_{CO_2} = 44$ g/mol and $M_{air} = 28.8$ g/mol.

The calibrations have been performed inside of the test section of the wind tunnel, to prevent the leakage of the CO_2 gas into the laboratory room. The nozzle (inner diameter 4 mm) for the calibration was set inside of the test section. The air is introduced to the nozzle through another small wind tunnel by the blower. The CO_2 gases of five different volumetric concentrations of 20%, 40%, 60%, 80% and 100% are introduced to the nozzle through the pressure control valve, the flow meter, and the rubber tube from the high pressure gas tanks. The temperature of CO_2 gas was adjusted to the same temperature as the air flow. The configuration of the present two-hot-wire probe is shown in Fig. 2. The two-hot-wire probe consists of the tungsten wire and the platinum wire (each wire diameter $d = 5$ μm; sensor length about 1 mm). The platinum wire probe can be operated at the large OHR because of its resistance to oxidation. The distance between the two wires is about 0.5 mm. The crucial length for the spatial resolution is the length of the wire sensor, i.e., 1 mm. So the resolution volume of the present probe can be considered to be 1.0^3 mm^3. As to the dynamic behavior of the hot wire, the measurement system by each wire sensor has the actual frequency response over 10 kHz. This is enough to measure the velocity and concentration fluctuation in the ordinary turbulent flows. Fig. 3 shows the examination results on the dependency of the relation between the platinum wire voltage E and the velocity U on OHR ε_R. In this figure, the OHR is based on the resistance of the wire, and may be defined as follows:

$$\varepsilon_R = (R_w - R_0)/R_0. \tag{11}$$

We note that ε_R is simply related to ε_T as $\varepsilon_T = \varepsilon_R/(bT_0)$. In comparison with Fig. 1, it is found that the results in Fig. 3 show qualitatively the same tendency as ones in Fig. 1. This fact seems to be important as the basis for adopting Eq. (6) to predict the hot-wire voltages with different OHRs in the CO_2 and air flows. We also find that at $\varepsilon_R = 0.7$ the wire voltages in the air and the CO_2 gas flows show approximately the same values.

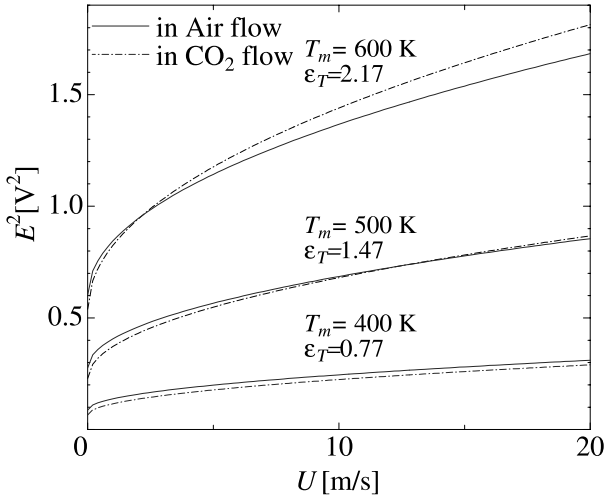

Fig. 1. Predction of the wire output voltages.

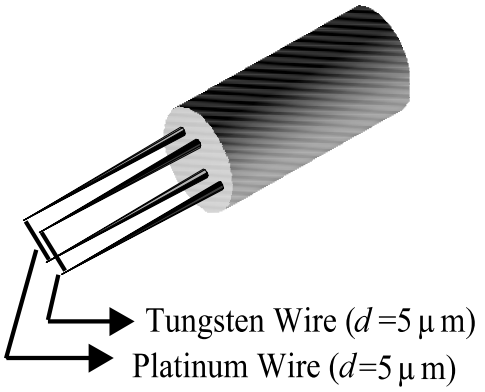

Fig. 2. Sketch of two-sensor hot-wire probe.

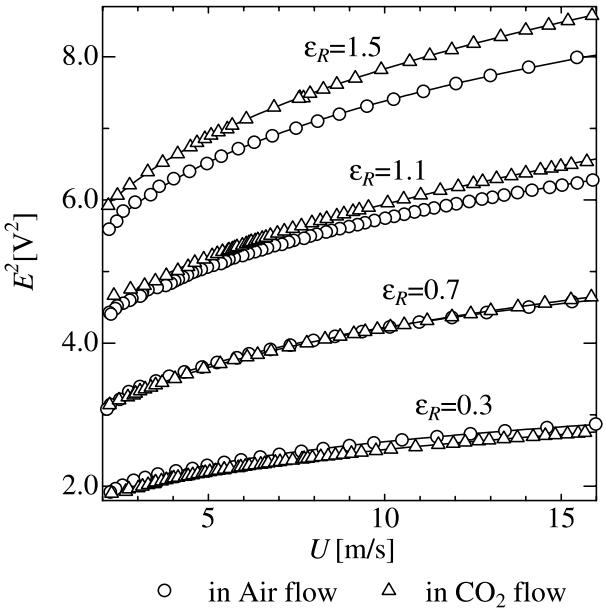

Fig. 3. $E^2 - U$ relations for different values of ε_R.

Figs. 4(a) and (b) show the calibration results for the gas mixture (CO_2–air) flow with several different CO_2 concentrations. Fig. 4(a) is the result for the tungsten wire in the case of $\varepsilon_R = 0.3$ and Fig. 4(b) is the result for the platinum wire in the case of $\varepsilon_R = 1.4$. It is found that as the concentration becomes large at the constant flow velocity, the wire voltage becomes gradually small at $\varepsilon_R = 0.3$ (Fig. 4(a)); conversely, however, it gradually becomes larger at $\varepsilon_R = 1.4$ (Fig. 4(b)). Later on (in Section 2.5), we will show that the above reversal phenomenon of the dependency of the wire voltage on the concentration is important to realize the high accuracy of the measurements.

2.4. Improved technique for simultaneous measurements of concentration and velocity

Chassaing (1979) reported that the appropriate adjustment of OHR makes it possible to measure the velocity of air–CO_2 mixture independently of the CO_2 concentration. However, seeing the details of the calibration curves for the air and CO_2 gas flows at $\varepsilon_R = 0.7$ in Fig. 3, which shows the best coincidence with each other, we still observe some deviation between the two curves. So it seems to be difficult to realize the complete coincidence of the curve for the air flow with that for the CO_2 gas flow. Even if it could be done, the appropriate adjustment of the OHR in every experiment is an enormous task indeed. So we conclude that the Chassaing's method give us some practical difficulty. Here we will propose a new simple measurement technique for simultaneous measurements of the concentration and velocity. This new method is described as follows.

Fig. 5 shows the relation between E_1^2 (E_1: tungsten wire voltage at small OHR $\varepsilon_R = 0.3$) and E_2^2 (E_2: platinum wire voltage at large OHR $\varepsilon_R = 1.4$), which is obtained from Figs. 4(a) and (b). In the figure, the solid lines are the curves for the constant concentration and the dashed lines those for constant velocity. By using the graph shown in Fig. 5, we can determine the concentration and velocity uniquely from a pair of E_1 and E_2. For the actual simultaneous measurements of concentration and velocity in a CO_2 jet, if we draw the graph like Fig. 5 beforehand, the instantaneous concentration and velocity for the pairs (E_1, E_2) can be calculated from this graph. The above

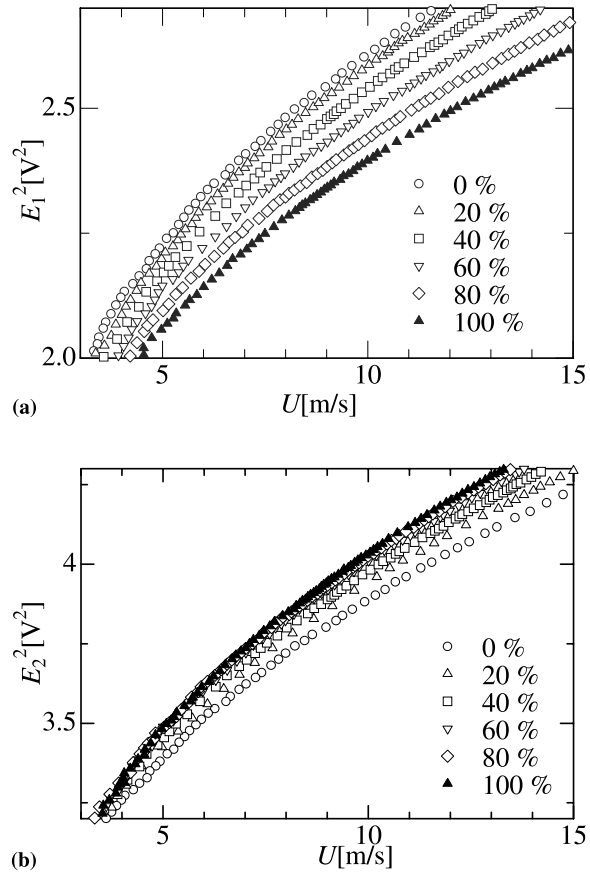

Fig. 4. Calibration curves for gas mixture (CO_2–air) flow: (a) $\varepsilon_R = 0.3$; (b) $\varepsilon_R = 1.4$.

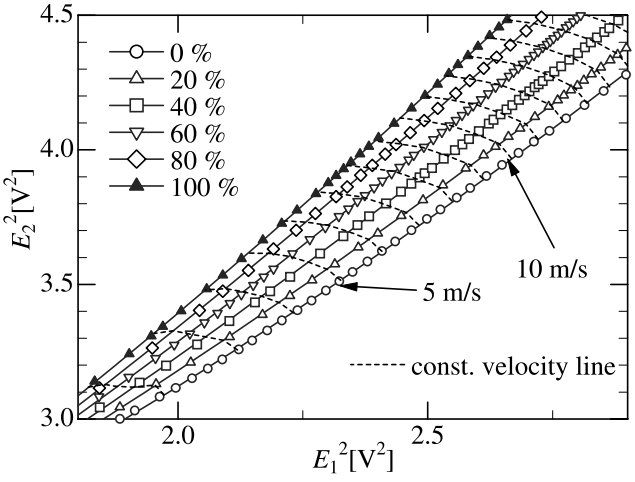

Fig. 5. Calibration map.

is an idea of the new method that we propose here. The graph shown in Fig. 5 is referred to as 'calibration map'.

2.5. Relation between measurement accuracy and dependency of calibration curve on concentration

In Section 2.3, it was found that the dependency of the $E^2 - U$ curve on the concentration is reversed with the change

of OHR. In this section, we investigate how the concentration dependency of the $E^2 - U$ curve is related to the measurement accuracy.

We now consider the transformation between the $(E_1^2,\ E_2^2)$ plane and (U, Γ) plane. As shown in Fig. 6, an infinitesimal element da on the $(E_1^2,\ E_2^2)$ plane is transformed into the element $d\bar{a}$ in the (U, Γ) plane. da can be related to $d\bar{a}$ as follows:

$$\mathrm{d}a = \frac{\partial(E_1^2, E_2^2)}{\partial(U, \Gamma)}\mathrm{d}\bar{a} = |J|\ \mathrm{d}U\ \mathrm{d}\Gamma, \tag{12}$$

where $J = \partial(E_1^2, E_2^2)/\partial(U, \Gamma)$ is the Jacobian for the transformation. J is given by

$$J = \frac{\partial(E_1^2, E_2^2)}{\partial(U, \Gamma)} = \begin{vmatrix} \dfrac{\partial E_1^2}{\partial U} & \dfrac{\partial E_1^2}{\partial \Gamma} \\ \dfrac{\partial E_2^2}{\partial U} & \dfrac{\partial E_2^2}{\partial \Gamma} \end{vmatrix} = \frac{\partial E_1^2}{\partial U}\frac{\partial E_2^2}{\partial \Gamma} - \frac{\partial E_1^2}{\partial \Gamma}\frac{\partial E_2^2}{\partial U}. \tag{13}$$

Consequently, we obtain

$$\mathrm{d}a = \left|\frac{\partial E_1^2}{\partial U}\frac{\partial E_2^2}{\partial \Gamma} - \frac{\partial E_1^2}{\partial \Gamma}\frac{\partial E_2^2}{\partial U}\right| \mathrm{d}U\ \mathrm{d}\Gamma. \tag{14}$$

From Eq. (14), it is found that the good sensitivity or the high accuracy of the measurements can be obtained when da is large, i.e., $|J|$ is large. Since $\partial E_1^2/\partial U > 0$ and $\partial E_2^2/\partial U > 0$ for the flows of the common gases and air, the large value of $|J|$ can be realized when $\partial E_1^2/\partial U < 0$ and $\partial E_2^2/\partial U > 0$ or $\partial E_1^2/\partial U > 0$ and $\partial E_2^2/\partial U < 0$. These situations correspond to the case in which the dependency of the wire voltage on the concentration is reversed between low and high OHRs. For the CO_2 and air flows, the above situation is actually realized, and this fact is one of the reasons why the two-sensor hot-wire probe is useful for the simultaneous measurements of concentration and velocity for the CO_2–air mixture flow.

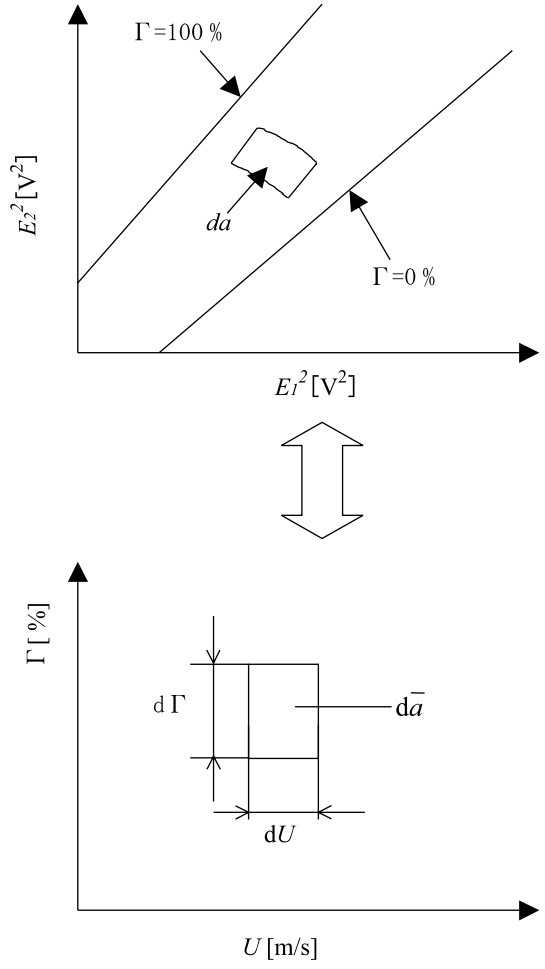

Fig. 6. Transformation between (E_1, E_2) plane and (Γ, U) plane.

2.6. Conversion of voltage pairs (E_1, E_2) to instantaneous concentration and velocity

With the new method proposed in Section 2.4, the conversion of the instantaneous wire voltage pairs to the simultaneous concentration and velocity was performed. Here we show an example using the data obtained at the centerline ($x/d_{\mathrm{eff}} = 15.0$, d_{eff} is the effective diameter of the jet exit (which will be defined in Section 3.1)) of a CO_2 jet. The sampling frequency is 10 kHz (experimental conditions will be described in detail in Section 3). Fig. 7 shows an example of the scattering plots of instantaneous voltage pairs (E_1, E_2) (corresponding to 0.04 s, 400 points) on (E_1, E_2) plane. The conversion of the two instantaneous voltage pairs (E_1, E_2) to the instantaneous concentration and velocity is carried out by the following method. Firstly, the calibration curves in Figs. 4(a) and (b) and the constant concentration curves in Fig. 5 are approximated by fifth-order polynomials. Next, in the region which contains all the measuring points, we generate a grid composed of 50 vertical lines (at a constant interval) and six constant concentration curves. The total number of grid points is 300 (50×6). Thirdly, we calculate the data of concentration and velocity on the grid points using the previous approximation polynomials for the calibration curves and the constant concentration curves. Finally, the concentration and velocity corresponding to the instantaneous voltage pair (E_1, E_2) are determined by the parametric spline surface interpolation method (Sugano et al., 1993) on the basis of the data on the grid points. Examples of the converted concentration and velocity signals are shown in Fig. 8. Here we should note that the concentration signal shown in Fig. 8 is for the volumetric concentration. The signal of the mass fraction concentration can be obtained digitally by the simple algebraic transformation given by Eq. (10).

3. Simultaneous measurements of concentration and velocity

3.1. Experimental conditions and method

The experiments have been performed in case of the CO_2 jet (the initial concentration $\Gamma_J = 100\%$) issuing into the grid turbulence. The grid mesh size M is 15 mm and the diameter of

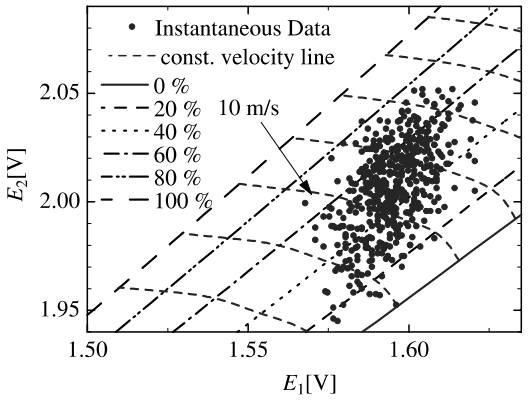

Fig. 7. Scattering plots of (E_1, E_2).

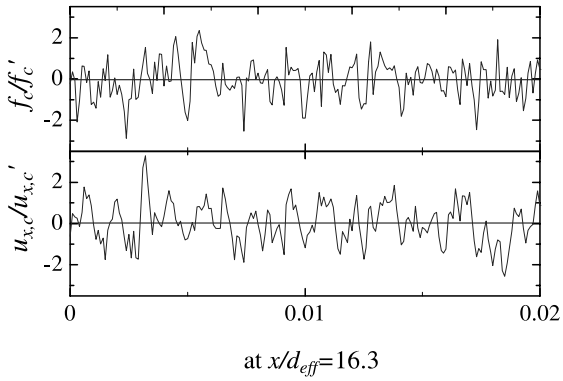

Fig. 8. Converted concentration and velocity signals.

the grid rod d_M is 3 mm. The sketch of the experimental equipment is shown in Fig. 9. The CO_2 gas can be introduced to the center of the grid from the gas tank through the pipe with which one of grid rods is replaced. Further the straight pipe (the outer diameter $d_{out}^{p} = 3.2$ mm, the inner diameter $d_{in}^{p} = 3$ mm) is set up in the downstream direction from the center of the grid. This straight pipe was connected to the short pipe attached to the center of the grid by the rubber tube (the outer diameter $d_{out} = 3.5$ mm, the inner diameter $d_{in} = 3$ mm). The CO_2 gas can be issued from the exit of this straight pipe of $d_{in}^{p} = 3$ mm into the grid turbulent flow. The exit of the issuing pipe is located at 150 mm ($15M$) downstream from the center of grid. With regard to the coordinate system for the jet, we set the cylindrical coordinates (x, r), where x and r are the axial and radial coordinates, respectively. The origin of the coordinate system is at the pipe exit.

The experimental conditions are as follows: the grid Reynolds number ($Re_M = U_0 M/\nu_{air}$) is 7000 (main velocity U_0 is about 7 m/s), the issuing Reynolds number of the CO_2 jet Re ($= (U_{x,J} - U_0)d_{in}^{p}/\nu_{CO_2}$) is 4600 (issuing velocity from pipe exit, $U_{x,J} = 18$ m/s; pipe exit diameter, $d_{in}^{p} = 3$ mm). The measurements have been made along the jet centerline and in the radial direction at the three different locations downstream of the pipe exit, i.e., at $x/d_{eff} = 13.7$, 27.3, 41.0 (d_{eff} is the effective diameter defined by $d_{eff} = d_{in}^{p}(\rho_J/\rho_0)^{0.5}$, where ρ_J is the issued fluid density, ρ_0 is the ambient fluid density). d_{eff} is 3.66 mm in the present experiments.

3.2. Experimental results

3.2.1. Decay of velocity fluctuation intensity in grid turbulence

Fig. 10 shows the downstream variations in the velocity fluctuation intensity in the grid turbulence with other experimental results. It is well known that intensity of turbulent velocity fluctuation decays in the downstream direction according to the power law. The power law is expressed as follows:

$$u'^2/U_0^2 = A(X/M - X_M/M)^{-n}, \tag{15}$$

where u' denotes the r.m.s. fluctuation intensity of the main streamwise velocity component, X is the downstream distance from the grid, A is a constant, n is the decaying power and X_M is the downstream distance of the virtual origin from the grid. In the present experiments, $A = 0.034$, $X_M = 1.0M$ and $n = 1.34$. Earlier results (Sreenivasan et al., 1980; Warhaft, 1984; Nakamura et al., 1987) shown in Fig. 10 give values of n between 1.2 and 1.45. The present result $n = 1.34$ is also within this range.

3.2.2. Simultaneous measurements of concentration and velocity in CO_2 jet

Variation of the mean mass fraction concentration and the difference between the mean axial velocity and the main stream velocity along the jet centerline are plotted as F_c/F_J and $(U_{x,c} - U_0)/(U_{x,J} - U_0)$ vs. x/d_{eff} in Figs. 11(a) and (b).The reciprocals of these quantities are also shown in the figures. From these figures, it is found that F_c and $(U_{x,c} - U_0)$ are inversely proportional to the downstream distance x in the regions of $x/d_{eff} \geqslant 5$ and $x/d_{eff} \geqslant 14$, respectively. The least-square linear fits are given by

$$\frac{F_J}{F_c} = 0.059\left(\frac{x}{d_{eff}} + 14.1\right), \tag{16}$$

$$\frac{(U_{x,c} - U_0)}{(U_{x,J} - U_0)} = 0.170\left(\frac{x}{d_{eff}} - 2.11\right). \tag{17}$$

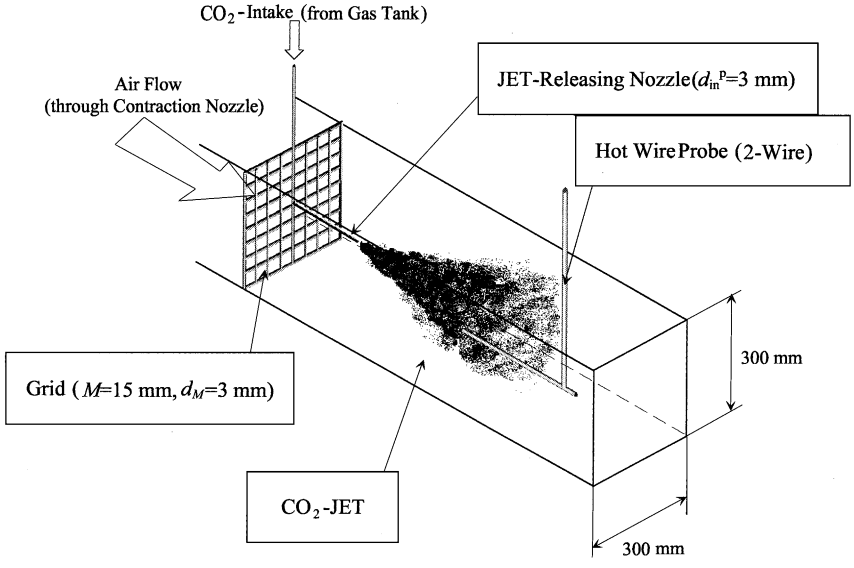

Fig. 9. Sketch of test section.

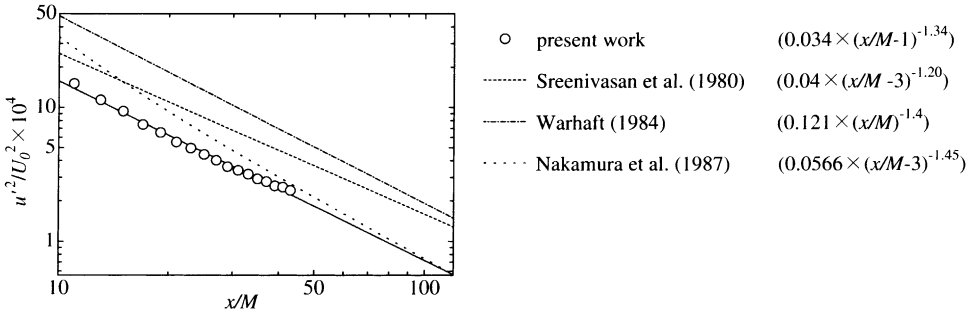

Fig. 10. Downstream variation of velocity fluctuation intensity in grid turbulence.

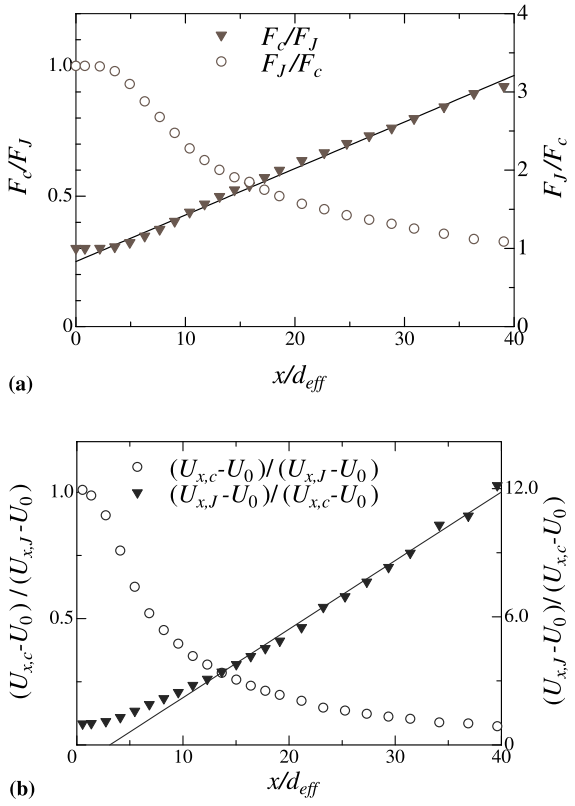

Fig. 11. Variation in mass fraction concentration F_c and the mean velocity difference $U_{x,c} - U_0$ along the jet centerline: (a) F_c/F_J, F_J/F_c vs. x/d_{eff}; (b) $(U_{x,c} - U_0)/(U_{x,J} - U_0)$, $(U_{x,J} - U_0)/(U_{x,c} - U_0)$ vs. x/d_{eff}.

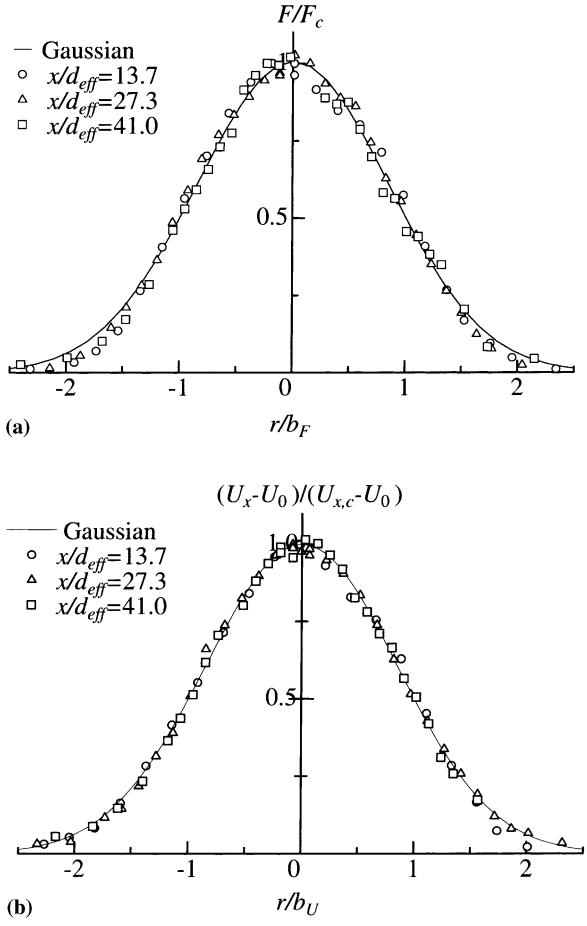

Fig. 12. Radial profiles of mean mass concentration and mean radial velocity difference: (a) F/F_c; (b) $(U_x - U_0)/(U_{x,c} - U_0)$.

Figs. 12(a) and (b) show the radial profiles of the mean mass fraction F and the mean axial velocity difference $U_x - U_0$ at three downstream locations. In these figures, b_F and b_U denote the halfwidths of the radial profiles of F and $U_x - U_0$, respectively. Both show a good similarity and agree very well with Gaussian distribution.

Centerline distributions of the mass fraction fluctuation r.m.s. intensity f'_c and the radial velocity fluctuation r.m.s. intensity $u'_{x,c}$ are shown in Figs. 13(a) and (b). f'_c and $u'_{x,c}$ are normalized by F_J and $U_{x,J} - U_0$, respectively, and the reciprocals of these quantities are also plotted in the figures. It is found that the reciprocal of f'_c increases linearly in the region of $x/d_{eff} \geqslant 15$. The best fit to the data for $x/d_{eff} \geqslant 15$ is given by

$$\frac{F_J}{f'_c} = 0.137\left(\frac{x}{d_{eff}} + 36.5\right). \tag{18}$$

The reciprocal of $u'_{x,c}$ shows also good linearity in the region of $x/d_{eff} \geqslant 10$. The linear fit is given by

$$\frac{U_{x,J} - U_0}{u'_{x,c}} = 0.170\left(\frac{x}{d_{eff}} + 13.6\right). \tag{19}$$

Figs. 14(a) and (b) show the radial profiles of the r.m.s. mass fraction intensity f' and the r.m.s. axial velocity u'_x. In the figure, f' and u'_x are normalized by the centerline values f'_c and $u'_{x,c}$, respectively. The peaks at the radial position are away from the jet centerline, and this tendency agrees with the past data in other reports (e.g., Becker et al., 1967; Panchapakesan and Lumley, 1993a,b).

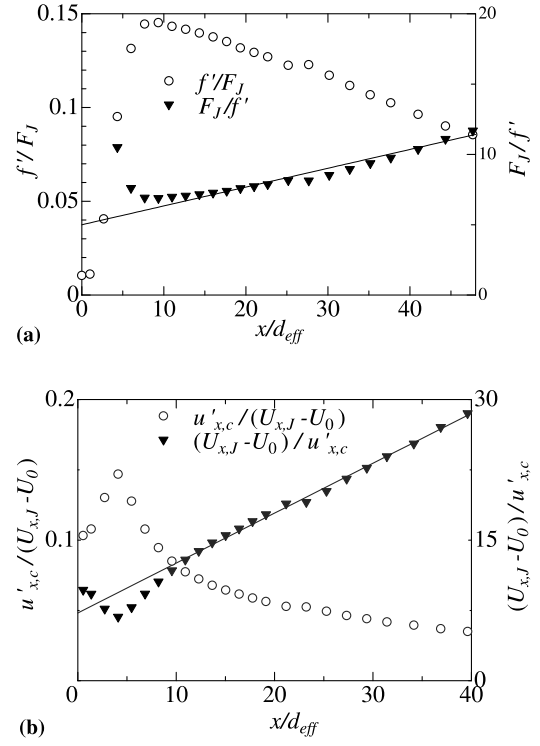

Fig. 13. Centerline variation in r.m.s. intensity of mass fraction concentration and axial velocity fluctuation: (a) mass fraction concentration intensity f_c'/F_J, and its reciprocal F_J/f_c'; (b) axial velocity intensity $u_{x,c}'/(U_{x,J}-U_0)$, and its reciprocal $(U_{x,J}-U_0)/u_{x,c}'$.

Fig. 15 shows the centerline variation of the axial turbulent scalar flux. In the figure, the scalar flux $\langle f_c u_{x,c}\rangle$ is normalized by $F_c U_{x,c}$, and the variation of $(F_J U_{x,J}/\langle f_c u_{x,c}\rangle)^{0.5}$ is also plotted. We find that $(F_J U_{x,J}/\langle f_c u_{x,c}\rangle)^{0.5}$ changes linearly in the downstream region of $x/d_{\mathrm{eff}} \geqslant 6.0$. Considering this linearity and the downstream variations of F_c and $U_{x,c}$, we conclude that the gradient type of diffusion model for the axial turbulent scalar flux is valid in this region (Sakai et al., 1999). The radial profiles of $\langle f u_x\rangle/(F_c U_{x,c})$ at $x/d_{\mathrm{eff}} = 13.7$, 27.3, 41.0 shown in Fig. 16 have an almost similar profile. Those radial profiles have peaks near $r/b_U = 0.6$, then decline to 0 in the outer region of the jet. This tendency agrees with the results for mass flux (helium gas) by Panchapakesan and Lumley (1993b) and for heat flux by Chevray and Tutu (1978) and Pietri et al. (2000).

Now the present results of radial profiles of f'/f_c', $u_x'/u_{x,c}'$ and $\langle f u_x\rangle/(F_c U_{x,c})$ are compared in more detail with other previous results. As shown in Fig. 14(a), the present data of f'/f_c' at $x/d_{\mathrm{eff}} = 13.7$ and 27.3 are close to the profile of the smoke jet (issuing Reynolds number of the jet $Re = 54{,}000$; the measurement range $20 \leqslant x/d \leqslant 36$, where d is the diameter of the jet exit) by Becker et al. (1967), but a little smaller values are observed at $x/d_{\mathrm{eff}} = 41.0$. On the other hand, the profile of helium jet ($Re = 3620$; $50 \leqslant x/d \leqslant 120$) by Panchapakesan and Lumley (1993b) is obviously different from the present data and ones by Becker et al. (1967). The reason of this difference may be related to the buoyancy effect. Before discussing the higher moments of turbulence quantities, the influence of buoyancy on the mean quantities should be addressed. Following Chen and Rodi (1976), the downstream extent of the inertial region of the jet is given by

$$x_{\mathrm{in}}/d = 0.5|Fr|^{1/2} R_\rho^{1/4}, \tag{20}$$

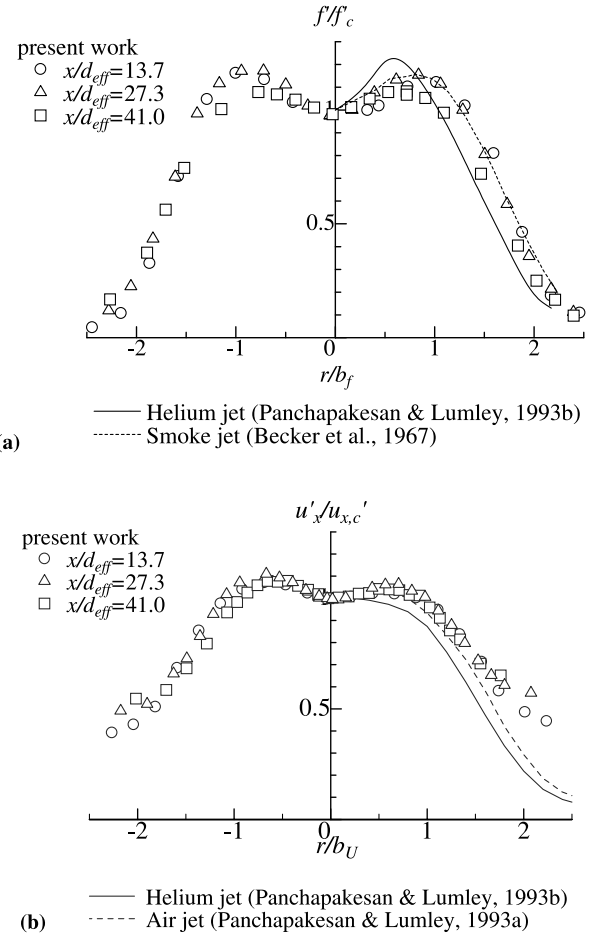

Fig. 14. Radial profiles of r.m.s. mass fraction concentration intensity and r.m.s. axial velocity intensity: (a) f'/f_c'; (b) $u_x'/u_{x,c}'$.

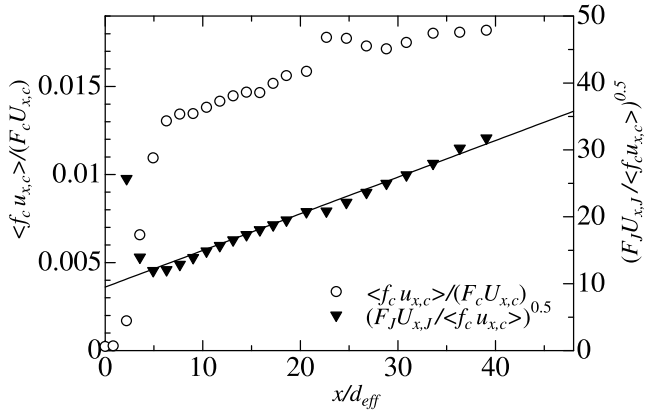

Fig. 15. Downstream variation in axial turbulent scalar flux.

where $Fr = U_{x,J}^2/\{(R_\rho - 1)gd\}$, $R_\rho = \rho_J/\rho_0$. The present condition is $Fr = 22{,}000$ and $R_\rho = 1.52$, then $x_{\mathrm{in}}/d = 82.3$ ($x/d_{\mathrm{eff}} = 63.4$). It is found that the present measurement range of $x/d_{\mathrm{eff}} \leqslant 41.0$ is within the inertial region, so that we expect no influence of buoyancy on the characteristics of mean quantities. On the other hand, as to the influence of buoyancy on the characteristics of turbulence quantities, e.g., $\langle f^2\rangle$, there seems to be no criterion such as Eq. (20). Consequently, the

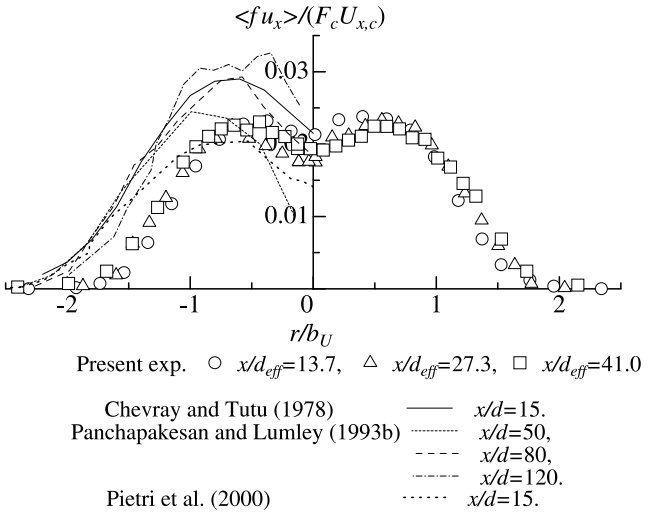

Fig. 16. Radial profiles of axial turbulent scalar flux.

similarity of $\langle f^2\rangle$ profile should be considered on the basis of the transport equation of $\langle f^2\rangle$ (Panchapakesan and Lumley, 1993b), which is given by

$$(\mathbf{U}\cdot\nabla)\cdot\langle f^2\rangle + 2\langle f\mathbf{u}\rangle\cdot\nabla F + \{\nabla\langle f^2\mathbf{u}\rangle + \langle f^2\mathbf{u}\rangle\cdot\nabla\langle p\rangle/\langle\rho\rangle\} = -2\varepsilon_f - c\langle\rho\rangle\{\langle f^2\mathbf{u}\rangle\cdot\nabla F + 4D_m\langle f\nabla f\otimes\nabla f\rangle\}, \quad (21)$$

where the flow and diffusion field are assumed to be steady, D_m is the molecular diffusivity, $\varepsilon_f = D_m\langle\nabla f\cdot\nabla f\rangle$, $c = (1/\rho_J) - (1/\rho_0)$, and the effects of variable density are represented by the term preceded by the factor $c\langle\rho\rangle$ (the second term on the right-hand side; this term is referred to the variable-density term (Panchapakesan and Lumley, 1993b)). From Eq. (21), it is found that the profile of $\langle f^2\rangle$ is influenced complexly by the second moment $\langle fu\rangle$, triple moment $\langle f^2u\rangle$, ∇F, $\nabla\langle\rho\rangle$, ε_f and the variable-density term. One of causes of the smaller values of f'/f'_c at $x/d_{\text{eff}} = 41.0$ for the present results in Fig. 14(a) seems to be the effect of buoyancy on the downstream changes of the above various mean and turbulence quantities. It should be noted that besides the buoyancy effect there may be other causes of the smaller values of f'/f'_c at $x/d_{\text{eff}} = 41.0$, for instance, the emission condition of the jet, the existence of the coflowing stream, the turbulence in the coflowing stream, the issuing Reynolds number. At present it is not clear which is most significant to the change of the f'/f'_c profile. The examination of the causes is our future important subject.

Next, we consider the results of Panchapakesan and Lumley (1993b) in Fig. 14(a). Their experimental condition is $Fr = 14{,}000$ and $R_\rho = 0.14$, then $x_{\text{in}}/d = 36.2$ from Eq. (20). Since their measurement range is $50 \leqslant x/d \leqslant 120$, this range is obviously out of the inertial region. In this case, the effect of buoyancy cannot be negligible even on the mean quantities. So it can be concluded that the reason of the big difference of the profile by Panchapakesan and Lumley (1993b) from the present data and ones by Becker et al. (1967) is the influence of buoyancy.

The buoyancy effect is also important to the radial profile of $u'_x/u'_{x,c}$ shown in Fig. 14(b). Panchapakesan and Lumley (1993b) found that in their experiments of helium jet the values of u'_x are higher than the air jet values in the fully turbulent region near the axis of the jet because of the buoyancy effect. So when u'_x is normalized by the value on the jet axis in the helium jet, the profile of $u'_x/u'_{x,c}$ become smaller than the one of air jet. On the other hand, in the present experiments $R_\rho = 1.52$. This value of R_ρ gives no significant effect on the u'_x profile, so that the present profile of $u'_x/u'_{x,c}$ agrees with the one of air jet near the jet axis. However, we observe still the difference between the present data and the profile of the air jet near the outer edge of the jet. This difference is because there exists the turbulence fluctuation in the coflowing stream in the present experiments.

Next, the radial profiles of $\langle fu_x\rangle/(F_cU_{x,c})$ shown in Fig. 16 are considered. The values of the present experiments are significantly different from ones by Panchapakesan and Lumley (1993b) (helium jet), Chevray and Tutu (1978) (heated jet) and Pietri et al. (2000) (heated jet). Here it should be noticed that the results by Chevray and Tutu (1978) and Pietri et al. (2000) also differ with each other, though the heated jet was investigated in both cases. Pietri et al. (2000) explained that the reason of the above difference is related to the emission condition of the jets, laminar for the case of the Chevray and Tutu (1978) and fully turbulent for their experiments, which influence the development of the various turbulent quantities in the jets. It is expected that the initial turbulence lead to the enhancement of the mixing and to the decrease of $\langle fu_x\rangle$. In our experiments, the jet was issued in the condition of fully developed turbulence from the pipe. This is probably the reason why our data are different from the profiles by Chevray and Tutu (1978) and Pietri et al. (2000). With regard to the results of Panchapakesan and Lumley (1993b), the buoyancy effect becomes significant as explained before, so that the values of $\langle fu_x\rangle$ increase with x/d in the central region of the jet. To understand the above change of $\langle fu_x\rangle$ profile, the detailed examination of the transport equation of $\langle f\mathbf{u}\rangle$ is essential. This seems to be one of very important subjects on the turbulent transport phenomena (Panchapakesan and Lumley, 1993b).

4. Conclusions

Hot-wire anemometry with good frequency response is applied to simultaneous measurements of fluctuating mass fraction concentration and velocity in CO_2–air mixtures. Using the calibration map, one can determine the instantaneous volumetric concentration and velocity from the voltages of two hot-wire sensors with different OHRs. The instantaneous mass fraction concentration can be obtained digitally by algebraic transformation (Eq. (10)). The simultaneous measurements of mass fraction concentration and axial velocity of the CO_2 jet issued into the grid turbulence were made. The centerline and radial distributions of the mean and r.m.s. values of mass fraction and velocity, and axial scalar flux are consistent with past data. Therefore, we conclude that the present method is useful for simultaneous measurements of fluctuating mass fraction concentration and velocity in turbulent CO_2–air mixtures.

References

Becker, H.A., Hottel, H.C., Williams, G.C., 1967. The nozzle-fluid concentration field of the round, turbulent, free jet. J. Fluid Mech. 30, 285–303.

Chassaing, P., 1979. Mélange turbulent de gaz inertes dans un jet tube libre. Thèse Doc. Sciences 42, Inst. Nat. Poly. de Toulouse.

Chen, C.J., Rodi, W., 1976. A review of experimental data of vertical turbulent buoyancy jets. IIHM Report No. 193, The University of Iowa.

Chevray, R., Tutu, N.K., 1978. Intermittency and preferential transport of heat in a round jet. J. Fluid Mech. 88, 133–160.

Collis, D.C., Williams, M.J., 1959. Two-dimensional convection from heated wires at low Reynolds numbers. J. Fluid Mech. 6, 357–384.

Katayama, K. (Chief Ed.), 1986. The Materials for the Heat Transfer Engineering, fourth ed. Japan Society of Mechanical Engineers, Tokyo, p. 329 (in Japanese).

Kramers, K., 1946. Heat transfer from sphere to flowing media. Physica 12, 61–80.

Nakamura, I., Sakai, Y., Miyata, M., 1987. Diffusion of matter by a non-buoyant plume in grid-generated turbulence. J. Fluid Mech. 178, 379–403.

Panchapakesan, N.R., Lumley, J.L., 1993a. Turbulence measurements in axisymmetric jets of air and helium. Part 1. Air jet. J. Fluid Mech. 246, 197–223.

Panchapakesan, N.R., Lumley, J.L., 1993b. Turbulence measurements in axisymmetric jets of air and helium. Part 2. Helium jet. J. Fluid Mech. 246, 225–247.

Pietri, L., Amielh, M., Anselmet, F., 2000. Simultaneous measurement of temperature and velocity fluctuations in a slightly heated jet combining a cold wire Laser Doppler Anemometry. Int. J. Heat Fluid Flow 21, 22–26.

Pitts, W.M., McCaffrey, B.J., 1986. Response behavior of hot wires and films to flows of different gases. J. Fluid Mech. 169, 465–512.

Sakai, Y., Okada, Y., Kobayashi, N., Nakamura, I., 1999. Measurements of velocity – scalar joint statistics in a high Schmidt number axisymmetric turbulent jet. In: Proceedings of the Third ASME/JSME Joint Fluids Engineering Conference, San Francisco, paper No. 7765, pp. 1–8.

Simpson, R.L., Wyatt, W.G., 1973. The behavior of hot-film anemometers in gas. J. Phys. E 6, 981–987.

Sreenivasan, K.R., Tavoularis, S., Henry, R., Corrsin, S., 1980. Temperature fluctuations and scales in grid-generated turbulence. J. Fluid Mech. 100, 597–621.

Sugano, K., Yoshimura, K., Takayama, F., 1993. Spline Interpolation by C (Data analysis/CG/Differential equations), Tokyo Denki University Press, pp. 68–98 (in Japanese).

Warhaft, Z., 1984. The interference of thermal fields from line sources in grid turbulence. J. Fluid Mech. 144, 363–387.

Warnatz, J., Maas, U., Dibble, R.W., 1999. Combustion – Physical and Chemical Fundamentals, Modeling and Simulation, Experiments, Pollutant Formation, second ed. Springer, Berlin, p. 2.

Way, J., Libby, P.A., 1971. Application of hot-wire anemometry and digital techniques to measurement in a turbulent helium jet. AIAA J. 9, 1567–1573.

Wu, P., Libby, P.A., 1971. Heat transfer to cylinders in helium and Helium–air mixtures. Int. J. Heat Mass Transfer 14, 1071–1077.